DNA-Functionalized Nanotube Membranes with Single-Base Mismatch Selectivity

Punit Kohli, C. Chad Harrell, Zehui Cao, Rahela Gasparac, Weihong Tan, Charles R. Martin*

We describe synthetic membranes in which the molecular recognition chemistry used to accomplish selective permeation is DNA hybridization. These membranes contain template-synthesized gold nanotubes with inside diameters of 12 nanometers, and a "transporter" DNA-hairpin molecule is attached to the inside walls of these nanotubes. These DNA-functionalized nanotube membranes selectively recognize and transport the DNA strand that is complementary to the transporter strand, relative to DNA strands that are not complementary to the transporter. Under optimal conditions, single-base mismatch transport selectivity can be obtained.

In both biology and technology, molecular recognition (MR) chemistry is used to selectively transport chemical species across membranes. For example, the transmembrane proteins that transport molecules and ions selectively across cell membranes contain MR sites that are responsible for this selective-permeation function (*1*–*3*). In a similar manner, MR agents such as antibodies have been incorporated into synthetic membranes so that the membranes will selectively transport the species that binds to the MR agent (*4*, *5*). However, there appear to be no previous examples of either biological or synthetic membranes where nucleic acid hybridization is used as the MR event to facilitate DNA or RNA transport through the membrane (*6*, *7*). If such membranes could be developed, they might prove useful for DNA separations and for the sensors needed, for example, in genomic research.

We describe synthetic MR membranes for selective DNA transport. We prepared these membranes by incorporating a "transporter" DNA, in this case a DNA-hairpin (*8*, *9*) molecule (Table 1), within the nanotubes of a gold nanotube membrane (*10*, *11*). We found that these membranes selectively recognized and transported the DNA molecule that was complementary to the transporter DNA. The rate of transport (flux) of the complementary strand was higher than the fluxes of permeating DNA molecules (Table 1) that contained as few as a single-base mismatch with the transporter DNA.

We prepared gold nanotube membranes with the template synthesis method (*12*), by electrolessly depositing gold along the pore walls of a polycarbonate template membrane (*10*, *11*). The template was a commercially available filter (Osmonics), 6 μm thick, with cylindrical, 30-nm-diameter pores and 6×10^8 pores per cm^2 of membrane surface area. The inside diameters of the gold nanotubes deposited within the pores of the template can be controlled by varying the deposition time. The membranes used here contained gold nanotubes with inside diameters of 12 ± 2 nm, as determined by a gas-flux measurement on three identical samples (*10*).

We chose a DNA hairpin (*8*, *9*) as our transporter strand. DNA hairpins contain a complementary base sequence at each end of the molecule (Table 1), and in an appropriate electrolyte solution, intramolecular hybridization causes a closed stem/loop structure to form. In order to form the duplex, the complementary strand must open this structure, and this is a competitive process in that the intramolecular hybridization that closes the stem must be displaced by hybridization of the complementary strand to the loop. As a result, hybridization can be very selective, and in optimal cases, single-base mismatch selectivity is observed (*8*, *9*). That is, the perfect complement hybridizes to the hairpin, but a strand containing even a single mismatch does not.

Our hairpin-DNA transporter (Table 1) was 30 bases long and contained a thiol substituent at the 5′ end that allowed it to be covalently attached to the inside walls of the gold nanotubes (*13*). The first six bases at each end of this molecule are complimentary to each other and form the stem of the hairpin, and the middle 18 bases form the loop (Table 1). The permeating DNA molecules were 18 bases long and were either perfectly complementary to the bases in the loop or contained one or more mismatches with the loop (Table 1). A second thiol-terminated DNA transporter was also investigated (Table 1). This DNA transporter was also 30 bases long, and the 18 bases in the middle of the strand were identical to the 18 bases in the loop of the hairpin-DNA transporter. However, this second DNA transporter did not have the complementary stem-forming bases on either end and thus could not form a hairpin. We used this linear-DNA transporter to test the hypothesis that the hairpin-DNA provides better transport selectivity because of its enhanced ability to discriminate the perfect-complement permeating DNA from the permeating DNAs that contained mismatches.

The transport experiments were done in a U-tube permeation cell (*10*) in which the gold nanotube membrane separated the feed half-cell containing one of the permeating DNA molecules (Table 1), dissolved in pH 7.2 phosphate buffer (ionic strength ~0.2 M), from the permeate half-cell that initially contained only buffer. We determined the rate of transport (flux) of the permeating DNA molecule from the feed half-cell through the membrane into the permeate half-cell by periodically measur-

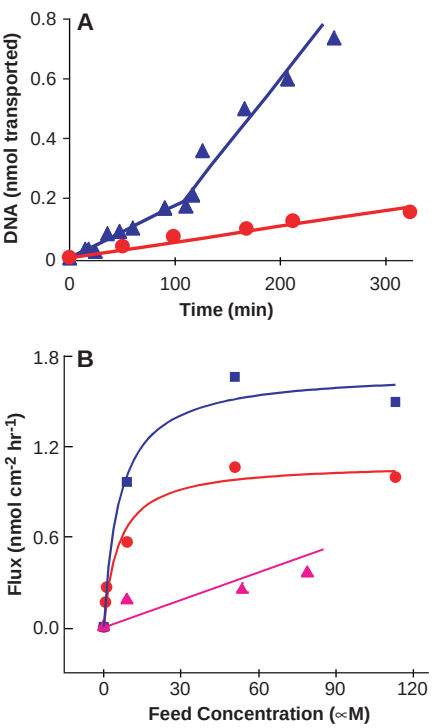

Fig. 1. (**A**) Transport plots for PC-DNA through gold nanotube membranes with (blue triangles) and without (red circles) the immobilized hairpin-DNA transporter. The feed solution concentration was 9 μM. (**B**) Flux versus feed concentration for PC-DNA. The data in red and blue were obtained for a gold nanotube membrane containing the hairpin-DNA transporter. At feed concentrations of 9 μM and above, the transport plot shows two linear regions. The data in blue (squares) were obtained from the high slope region at longer times. The data in red (circles) were obtained from the low slope region at shorter times. The data in pink (triangles) were obtained for an analogous nanotube membrane with no DNA transporter.

Department of Chemistry and Center for Research at the Bio/Nano Interface, University of Florida, Gainesville, FL 32611–7200, USA.

*To whom correspondence should be addressed. E-mail: crmartin@chem.ufl.edu

ing the ultraviolet absorbance of the permeate half-cell solution, at 260 nm, that arose from the permeating DNA molecule.

Transport plots (Figs. 1A and 2) show the number of nanomoles of the permeating DNA transported through the nanotube membrane versus permeation time. When the hairpin DNA was not attached, a straight-line transport plot was obtained for the perfect-complement DNA (PC-DNA) (Fig. 1A), and the slope of this line provides the flux of PC-DNA across the membrane (Table 2). The analogous transport plot for the membrane containing the hairpin-DNA transporter is not linear, but instead can be approximated by two straight-line segments: a lower slope segment at short times followed by a higher slope segment at times longer than a critical transition time, τ. This transition is very reproducible; for example, for a feed concentration of 9 μM, τ was 110 $\pm$ 15 min (average of three membranes).

Figure 1A shows that the flux of the permeating PC-DNA in the membrane containing the hairpin-DNA transporter was at all times higher than the flux for an otherwise identical membrane without the transporter (Table 2). Hence, the hairpin DNA acted as an MR agent to facilitate the transport (*4*, *5*, *14*, *15*) of the PC-DNA. Additional evidence for this conclusion was obtained from studies of the effect of concentration of the PC-DNA in the feed solution on the PC-DNA flux. If the hairpin DNA facilitated the transport of the PC-DNA, this plot should show a characteristic "Langmuirian" shape (*4*, *5*). Figure 1B shows that this is indeed the case, for transport data both before and after τ. The analogous plot for the identical membrane without the hairpin-DNA transporter is linear (Fig. 1B), showing that transport is not facilitated but rather described simply by Fick's first law of diffusion. The transition to the higher slope segment was not observed, during permeation experiments with a total duration of 300 min, for feed concentrations below 9 μM (Fig. 1B).

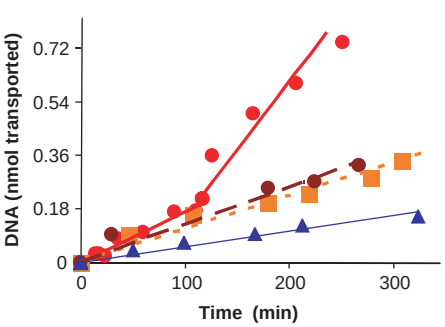

Fig. 2. Transport plots for a gold nanotube membrane containing the hairpin-DNA transporter. The permeating DNA was either PC-DNA (red circles), single-mismatch (end) (brown circles), seven-mismatch (blue triangles), or single-mismatch (middle) (orange squares). The feed solution concentration was 9 μM.

Analogous permeation data were obtained for the various mismatch-containing permeating DNA molecules (Table 1). The transport plots for these mismatch DNAs show only one straight-line segment (Fig. 2), and their fluxes were always lower than the flux for the PC-DNA obtained from the higher slope region of the PC-DNA transport plot (Table 2). In particular, the membrane containing the hairpin-DNA transporter showed higher flux for PC-DNA than for the two permeating DNAs that contained only a single-base mismatch.

To illustrate this point more clearly, we defined a selectivity coefficient $\alpha_{HP,PC/1MM}$, which is the flux for the PC-DNA divided by the flux for a single-base mismatch DNA in the membrane with the hairpin (HP)–DNA transporter. A selectivity coefficient of $\alpha_{HP,PC/1MM} = 3$ can be derived from the data in Table 1. The analogous selectivity coefficient for the PC-DNA versus the DNA with seven mismatches is $\alpha_{HP,PC/7MM} = 7$. These selectivity coefficients show that nanotube membranes containing the hairpin-DNA transporter selectively transport PC-DNA and that single-base mismatch transport selectivity can be obtained.

The importance of the hairpin structure to membrane selectivity is illustrated by analogous transport data for membranes containing the linear-DNA transporter (Table 1). With this transporter, all of the transport plots show only a single straight-line segment, and the fluxes for the single-mismatch DNAs were identical to the flux for the PC-DNA (Table 2); i.e., the single-base mismatch selectivity coefficient for this linear (LN) DNA transporter is $\alpha_{LN,PC/1MM} = 1$. The linear-DNA transporter does, however, show some transport selectivity for the PC-DNA versus the seven-mismatch DNA, $\alpha_{LN,PC/7MM} = 5$.

We also investigated the mechanism of transport in these membranes. In such MR-based, facilitated-transport membranes, the permeating species is transported by sequential binding and unbinding events with the MR agent (*4*, *5*, *14*). For these DNA-based membranes, the binding and unbinding events are sequential hybridization and dehybridization reactions between the permeating DNA molecule and the DNA transporter attached to the nanotubes. To show that hybridization occurred in the membrane with the hairpin-DNA transporter, the membrane was exposed to PC-DNA and then to a restriction enzyme (Sfc I, New England Biolabs) (*13*). If hybridization between the PC-DNA and the hairpin transporter occurs, this enzyme would cut the resulting double-stranded DNA such that the last five bases of the binding loop, and all of the stem-forming region, at the 3′ end of the hairpin would be removed. This reaction would substantially damage the binding site, and on the basis of our prior work (*4*), we predicted that if this membrane were subsequently used in a permeation experiment, a lower PC-DNA flux would be obtained (*16*).

After exposure to the restriction enzyme, the membrane was extensively rinsed to remove the enzyme and DNA fragments and was then

Table 1. DNA molecules used. For transporter DNAs, the 18 bases that bind to the permeating DNAs are in bold. For permeating DNAs, the mismatched bases are underlined. FAM is a fluorescein derivative (Applied Biosystems), and Cy5 is a cyanine dye (Amersham Biosciences).

Type	Sequence
Transporter DNAs	
Hairpin	5′HS-$(CH_2)_6$-CGCGAG**AAGTTACATGACCTGTAG**CTCGCG3′
Linear	5′HS-$(CH_2)_6$-CGCGAG**AAGTTACATGACCTGTAG**ACGATC3′
Permeating DNAs	
Perfect complement (PC-DNA)	3′TTCAATGTACTGGACATC5′
Single-base mismatch (3′ end)	3′C̲TCAATGTACTGGACATC5′
Single-base mismatch (middle)	3′TTCAATGTAG̲TGGACATC5′
Seven-mismatch	3′AAGTTACATGACCTGTAG5′
FAM-labeled perfect complement	3′TTCAATGTACTGGACATC-$(CH_2)_6$-FAM 5′
Cy5-labeled single-base mismatch	3′C̲TCAATGTACTGGACATC-$(CH_2)_6$ Cy5 5′

Table 2. Fluxes for a feed concentration of 9 μM.

Transporter DNA	Permeating DNA	Flux (nmol cm^{-2} h^{-1})
Hairpin	Perfect complement	0.57, 1.14*
Linear	Perfect complement	0.94
None	Perfect complement	0.20
Hairpin	Single mismatch (middle)	0.37
Hairpin	Single mismatch (end)	0.44
Linear	Single mismatch (middle)	0.94
Hairpin	Seven-mismatch	0.17
Linear	Seven-mismatch	0.20

*Two fluxes were obtained because the transport plot showed two slopes (Fig. 1A).

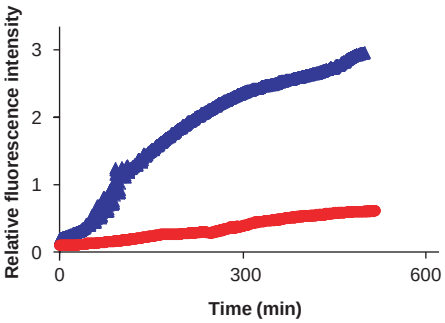

Fig. 3. Release of fluorescently labeled PC-DNA from a membrane containing the hairpin-DNA transporter. The fluorescently labeled PC-DNA was released into a buffer solution containing no unlabeled PC-DNA (lower curve) or into a buffer containing 9 μM unlabeled PC-DNA (upper curve).

used for a transport experiment with PC-DNA as the permeating species. Unlike the data in Fig. 1A, the transport plot for this damaged-transporter membrane showed only one straight-line segment (*13*), corresponding to a flux of 0.2 nmol cm^{-2} h^{-1}. This value is well below those we observed from membranes with an undamaged DNA-hairpin transporter (Table 2). The damaged DNA-transporter was then removed from the nanotubes, and fresh DNA-hairpin transporter was applied. A subsequent transport experiment with PC-DNA showed a transport plot identical to that obtained before exposure to the restriction enzyme (*13*). These data suggest that hybridization is, indeed, involved in the transport mechanism for the DNA-hairpin–containing membranes.

To show that dehybridization occurs on a reasonable time scale in these membranes, we exposed a hairpin-DNA membrane to a fluorescently labeled version of the PC-DNA (Table 1). The membrane was then rinsed with buffer solution and immersed into a solution of either pure buffer or buffer containing unlabeled PC-DNA. If the dehybridization reaction is facile, the fluorescently labeled PC-DNA should be released into the solution. We found that dehybridization did occur, but it was strongly accelerated when unlabeled PC-DNA was present in the solution (Fig. 3). Hence, dehybridization is much faster when it occurs through a cooperative process whereby one PC-DNA molecule displaces another from an extant duplex (*17*).

We also investigated transport selectivity for a feed solution containing fluorescently labeled versions (Table 1) of both the PC-DNA and the single-mismatch DNA. The fluorescent labels allowed for quantification of both of these permeating DNAs simultaneously in the permeate solution. In analogy to the single-molecule permeation experiment, the flux of the PC-DNA was five times higher than the flux of the single-mismatch DNA (*13*). To assess the practical utility of these membranes, transport studies with more realistic samples (such as cell lysates) will be needed.

Finally, we have not observed a spontaneous transition from a low-flux to a high-flux state (Fig. 1A) with our previous MR-based membranes (*4*, *5*). The fact that whether this transition is observed depends on the feed concentration suggests that the transition is a transport-related phenomenon. It is possible that this transition relates to the concept of cooperative (high-flux) versus noncooperative (low-flux) dehybridization (Fig. 3), but further studies, both experimental and modeling, will be required before a definitive mechanism for this transition can be proposed.

References and Notes

1. D. A. Doyle *et al.*, *Science* **280**, 69 (1998).
2. J. Abramson *et al.*, *Science* **301**, 610 (2003).
3. B. Hille, *Ion Channels of Excitable Membranes* (Sinauer, Sunderland, MA, ed. 3, 2001), pp. 441–470.
4. S. B. Lee *et al.*, *Science* **296**, 2198 (2002).
5. B. B. Lakshmi, C. R. Martin, *Nature* **388**, 758 (1997).
6. An interesting example of attaching a single-stranded DNA molecule to a protein channel to make a new type of DNA sensor has been reported (*18*).
7. H. Fried, U. Kutay, *Cell. Mol. Life Sci.* **60**, 1659 (2003).
8. G. Bonnet, S. Tyagi, A. Libchaber, F. R. Kramer, *Proc. Natl. Acad. Sci. U.S.A.* **96**, 6171 (1999).
9. B. Dubertret, M. Calame, A. J. Libchaber, *Nature Biotechnol.* **19**, 365 (2001).
10. C. R. Martin, M. Nishizawa, K. Jirage, M. Kang, *J. Phys. Chem. B* **105**, 1925 (2001).
11. K. B. Jirage, J. C. Hulteen, C. R. Martin, *Science* **278**, 655 (1997).
12. C. R. Martin, *Science* **266**, 1961 (1994).
13. Materials and methods are available as supporting material on *Science* Online.
14. M. Mulder, *Basic Principles of Membrane Technology* (Kluwer, Dordrecht, Netherlands, 1996), pp. 342–351.
15. Y. Osada, T. Nakagawa, in *Membrane Science and Technology*, Y. Osada, T. Nakagawa, Eds. (Marcel Dekker, New York, 1992), pp. 377–391.
16. A fluorescence-based method was used to provide direct evidence for clipping of the double-stranded DNA by the restriction enzyme (*13*).
17. M. C. Hall, H. Wang, D. A. Erie, T. A. Kunkel, *J. Mol. Biol.* **312**, 637 (2001).
18. S. Howorka, S. Cheley, H. Bayley, *Nature Biotech.* **19**, 636 (2001).
19. Supported by the National Science Foundation and by the Defense Advanced Research Projects Agency.

Supporting Online Material

www.sciencemag.org/cgi/content/full/305/5686/984/DC1
Materials and Methods
Figs. S1 to S3
References and Notes

6 May 2004; accepted 9 July 2004

Sample Dimensions Influence Strength and Crystal Plasticity

Michael D. Uchic,[1]* Dennis M. Dimiduk,[1] Jeffrey N. Florando,[2] William D. Nix[3]

When a crystal deforms plastically, phenomena such as dislocation storage, multiplication, motion, pinning, and nucleation occur over the submicron-to-nanometer scale. Here we report measurements of plastic yielding for single crystals of micrometer-sized dimensions for three different types of metals. We find that within the tests, the overall sample dimensions artificially limit the length scales available for plastic processes. The results show dramatic size effects at surprisingly large sample dimensions. These results emphasize that at the micrometer scale, one must define both the external geometry and internal structure to characterize the strength of a material.

A size-scale effect can be defined as a change in material properties—mechanical, electrical, optical, or magnetic—that is due to a change in either the dimensions of an internal feature or structure or in the overall physical dimensions of a sample. For metals, size-scale effects related to changes in internal length scales are readily observed and are often exploited for industrial use. For example, it is well known that the yield strengths of metallic alloys can be improved through refinement of the grain size (*1–3*), where the yield strength is proportional to the inverse square root of the average grain diameter, and this relation is generally valid for grains that range in size from millimeters to tens of nanometers. By comparison, changes in the mechanical response of materials due solely to the physical geometry of a sample have been largely overlooked. Large increases in yield strength (approaching the theoretical limit) were observed over 40 years ago in tension testing of single-crystal metallic whiskers having micrometer-scale diameters (*4–6*). However, whisker testing is restricted to materials that can be grown in that form. Conversely, no changes in strength and only mild decreases in work hardening were observed during the deformation of

[1]Air Force Research Laboratory, Materials & Manufacturing Directorate, Wright-Patterson Air Force Base, OH 45433–7817, USA. [2]Lawrence Livermore National Laboratory, Livermore, CA 94550, USA. [3]Department of Materials Science and Engineering, Stanford University, Stanford, CA 94305–2205, USA.

*To whom correspondence should be addressed. E-mail: michael.uchic@wpafb.af.mil